Volume 16
Number 1
7 January 2024
Pages 1-490

Nanoscale

rsc.li/nanoscale

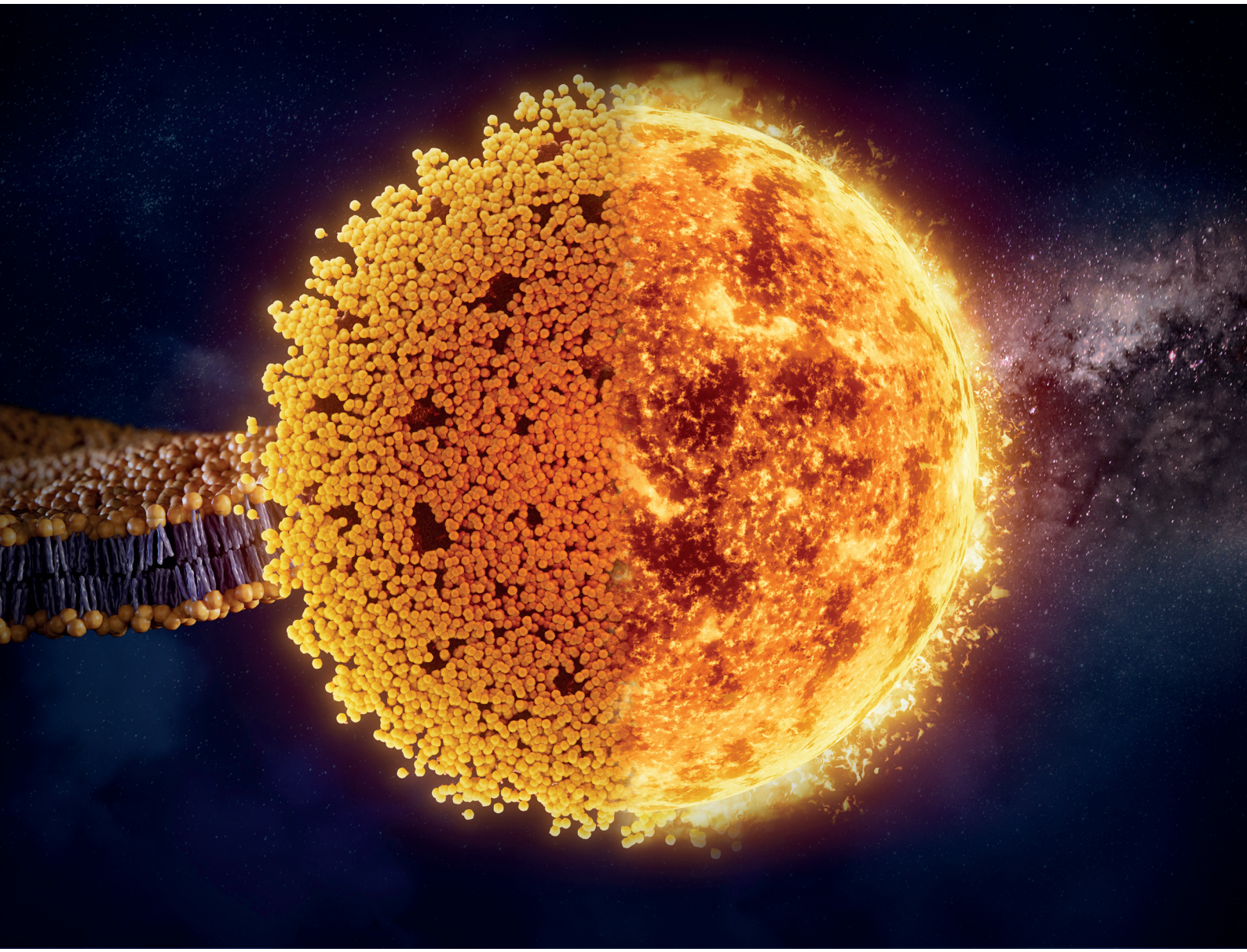

ISSN 2040-3372

ROYAL SOCIETY OF CHEMISTRY

PAPER
Emilia Krok, Lukasz Piatkowski *et al.*
Nanoscale structural response of biomimetic cell membranes to controlled dehydration

NCNST

Nanoscale

PAPER

View Article Online
View Journal | View Issue

Cite this: *Nanoscale*, 2024, **16**, 72

Nanoscale structural response of biomimetic cell membranes to controlled dehydration†

Emilia Krok, *[a] Henri G. Franquelim, [b,c] Madhurima Chattopadhyay, [a] Hanna Orlikowska-Rzeznik, [a] Petra Schwille [b] and Lukasz Piatkowski *[a]

Received 26th June 2023,
Accepted 15th November 2023

DOI: 10.1039/d3nr03078d

rsc.li/nanoscale

Although cell membranes exist in excess of water under physiological conditions, there are a number of biochemical processes, such as adsorption of biomacromolecules or membrane fusion events, that require partial or even complete transient dehydration of lipid membranes. Even though the dehydration process is crucial for understanding all fusion events, still little is known about the structural adaptation of lipid membranes when their interfacial hydration layer is perturbed. Here, we present the study of the nanoscale structural reorganization of phase-separated, supported lipid bilayers (SLBs) under a wide range of hydration conditions. Model lipid membranes were characterised using a combination of fluorescence microscopy and atomic force microscopy and, crucially, without applying any chemical or physical modifications that have previously been considered essential for maintaining the membrane integrity upon dehydration. We revealed that decreasing the hydration state of the membrane leads to an enhanced mixing of lipids characteristic of the liquid-disordered (L_d) phase with those forming the liquid-ordered (L_o) phase. This is associated with a 2-fold decrease in the hydrophobic mismatch between the L_d and L_o lipid phases and a 3-fold decrease in the line tension for the fully desiccated membrane. Importantly, the observed changes in the hydrophobic mismatch, line tension, and lipid miscibility are fully reversible upon subsequent rehydration of the membrane. These findings provide a deeper insight into the fundamental processes, such as cell–cell fusion, that require partial dehydration at the interface of two membranes.

1 Introduction

Biological cell membranes are permeable barriers responsible for maintaining homeostasis and protecting the cell from the surrounding environment.[1] They act as gateways, mediating the selective transport of ions and biomacromolecules such as glucose or amino acids.[2] They also play a key role in cell compartmentalisation, allowing mutually exclusive biochemical processes to occur simultaneously within the cell.[3] The study of cellular membranes in their native form is very challenging due to the high structural complexity of these systems and the plethora of chemical, biological and physical processes that occur within the cell. For this reason, model biological cell membranes are often used, such as giant unilamellar vesicles (GUVs) or supported lipid bilayers (SLBs), which have analogous physical and structural properties to native cell membranes, but at the same time can be modified and simplified to focus on specific biophysical properties.[4–9]

The lateral organisation of lipid membranes is driven by the interplay of lipid–lipid and lipid–protein interactions.[10] However, this biological system is not complete without water, the presence of which is considered to be an indispensable factor that modulates the structural organisation of membranes, phase separation, as well as the spatial arrangement of transmembrane proteins, both in model membrane systems and living cells.[11–13] Water acts on the membrane in particular in the presence of the so-called hydrophobic mismatch, which occurs when the thickness of different membrane constituents is different, leading to an exposure of the hydrophobic moieties to water.[14] This hydrophobic interaction is energetically unfavourable and is therefore one of the main mechanisms driving the phase separation.[15] García-Sáez *et al.* modified the thickness of the disordered phase using phosphatidylcholines with different acyl chain lengths and showed that the bigger the difference between the hydrophobic parts of the membrane, the stronger the phase separation, and the higher the

[a]*Poznan University of Technology, Faculty of Materials Engineering and Technical Physics, Institute of Physics, Piotrowo 3, 60-965 Poznan, Poland. E-mail: emilia.krok@put.poznan.pl, lukasz.j.piatkowski@put.poznan.pl*
[b]*Department of Cellular and Molecular Biophysics, Max Planck Institute of Biochemistry, Am Klopferspitz 18, 82152 Martinsried, Germany*
[c]*Leipzig University, Research and Transfer Center for Bioactive Matter, Deutscher Platz 5, 04103 Leipzig, Germany*

†Electronic supplementary information (ESI) available. See DOI: https://doi.org/10.1039/d3nr03078d

line tension at the boundary between the two phases.[16] Line tension is also responsible for the self-healing properties of the cell membranes by facilitating the closure of transient pores within the structure of the lipid bilayer.[17] Line tension for single component membranes can be determined by inducing the formation of transient pores in the membrane structure and observing the rate of pore closure. Srividya *et al.* showed that the line tension in single phase membranes increases with the acyl chain length of the constituting lipids.[18]

Although lipid membranes under natural conditions indeed exist in excess of water, there are biological processes that require at least partial interfacial dehydration of lipid bilayers. Processes such as endo- and exocytosis,[19] neurotransmission,[20] viral entry,[21] fertilization,[22] or cell fusion during embryogenesis[23] and morphogenesis[24] involve the fusion of two lipid membranes. All of these membrane fusion events rely on interactions between lipids, proteins, and water hydrating the two interfacing membranes.[25] When the two bilayers come in close contact and the distance between them is reduced to about 2–3 nm, a strong hydration repulsion, also known as the "hydration force", occurs between their hydrophilic surfaces.[26–28] At this stage the thin water layer separating the membranes must be expelled for hemi-fusion to occur.

Thus, to fully understand the intricate interactions between membrane constituents and the membrane hydration layer, as well as the biophysical consequences of these interactions, it is crucial to gain insight into the structural properties of cellular membranes when their hydration state is altered. Indeed, Chiantia *et al.* reported on the structure of SLBs composed of DOPC/SM/cholesterol under conditions of complete dehydration using atomic force microscopy (AFM).[29] They showed that in the absence of stabilising agents such as trehalose, the membranes lose their integrity upon abrupt dehydration and subsequent rehydration and severe structural damage is observed in the form of holes, aggregates and delimitation of membranes.[30] Similar results were reported by Iriarte-Alonso *et al.* for single-component DOPC membranes, where abrupt dehydration resulted in the formation of multiple defects and holes, and consequently loss of membrane continuity.[31] Many attempts have been made to preserve the structure of desiccated lipid membranes and prevent them from rapid vesiculation. These include the use of saccharides, which are known to increase the spacing between lipids in the dry state and thus prevent them from collapsing,[30,32] the modification of lipid head groups to improve the interactions between the lipids and the solid support[33–35] or the introduction of physical confinement, which prevents the interfacial peeling force from causing destructive membrane delamination.[36] All of these approaches, although successful in membrane preservation, involve alteration of the native properties of lipid membranes due to the introduced chemical or physical modifications of either the membrane or the solid support. Recently, we presented a novel method for membrane preservation under dehydration conditions based on the controlled steady decrease of environmental humidity, which provides new possibilities to study the behavior and properties of membranes without altering their chemical composition or physical features.[37,38]

In this study, we have used a combination of fluorescence and atomic force microscopy to investigate the nanoscale structural response of phase-separated SLBs to a wide range of hydration conditions. Our results demonstrate that the structure of lipid membranes can be preserved even under conditions of complete desiccation without the use of stabilising agents, if the dehydration process is carried out in a gradual and controlled manner. The dehydration method used here allowed the overall structural organisation of the membrane to be maintained without the appearance of defects or holes. At the same time, the removal of bulk water led to a prominent nanoscale structural reorganisation within the membrane. We observed that the dehydration process causes a significant decrease in the hydrophobic mismatch between the L_d and L_o phases, and consequently lowers the line tension at their interface. Importantly, this process is fully reversible and upon subsequent rehydration, the height mismatch increases to its initial state. We show that the removal of bulk water leads to an extensive mixing of the liquid-disordered (L_d) and liquid-ordered (L_o) phase lipids and changes in the borderline of the L_o phase domains. Finally, the present study employs a pioneering methodology of AFM measurements under controlled humidity, which can be applied to study other model cell systems under varying hydration conditions.

2 Materials and methods

2.1 Materials

1,2-Dimyristoleoyl-*sn-glycero*-3-phosphocholine (14 : 1 PC or DMoPC), egg yolk sphingomyelin (SM), and cholesterol were purchased from Avanti Polar Lipids, Alabaster AL., USA. Monosialoganglioside (GM1) from bovine brain, 1,2-dioleoyl-*sn-glycero*-3-phosphoethanolamine labeled with Atto 633 (DOPE-Atto 633), sodium hydroxide (NaOH), calcium chloride ($CaCl_2$), and sodium chloride (NaCl) were purchased from Merck KGaA, Darmstadt, Germany. Alexa Fluor 488 conjugated with a cholera toxin B subunit (CTxB-Alexa 488) was obtained from Molecular Probes, Life Technologies, Grand Island, NY, USA. *N*-2-Hydroxyethyl piperazine-*N*′-2-ethane sulphonic acid (HEPES PUFFERAN) was obtained from Carl Roth GmbH & Co KG, Karlsruhe, Germany. All the materials and reagents were used without further purification. Optical adhesive glue Norland 68 was purchased from Norland Products Inc., Cranbury, NJ, USA. Ultrapure water was obtained using a Milli-Q reference water purification system from Merck KGaA, Darmstadt, Germany.

2.2 Vesicles' preparation

Multilamellar vesicles (MLVs) were formed by dissolving DMoPC, SM, and cholesterol in chloroform in a 1 : 1 : 1 molar ratio with the addition of 0.1 mol% of DOPE-Atto 633 dye,

resulting in a 10 mM solution of the lipids. For the representative fluorescence imaging purposes 0.1 mol% of GM1 was added for further labelling with CTxB-Alexa 488. The lipid mixture was dried under nitrogen gas for 20 minutes, leaving a thin film of lipids deposited on the bottom of the vial. The dried lipid mixture was further desiccated in a vacuum dry chamber for at least 2 h to ensure the complete removal of the organic solvent. The lipids were resuspended in a buffer solution (10 mM HEPES and 150 mM NaCl, pH adjusted to 7.4 with NaOH) and subjected to four cycles of heating on a hot plate at 60 °C and vortexing. Each heating and vortexing step was performed for 1 min. 10 μL aliquots of the lipid suspension containing MLVs were distributed into new sterilised glass vials and stored at −20 °C until further use.

2.3 SLB preparation

SLBs were formed using a previously reported method.[39] Briefly, lipid vesicles were diluted 10 times to a final lipid concentration of 1 mM by addition of HEPES buffer. Aliquots containing MLVs were sonicated in a Bransonic 1800 ultrasonic bath for 10 min to generate small unilamellar vesicles (SUVs). To prepare a solid support for lipid deposition, a thin layer of freshly cleaved mica was glued using UV-activated glue onto a round glass coverslip. A half-cut 2 ml Eppendorf tube was placed on top of the coverslip and sealed with silicone to provide a temporary water reservoir necessary for SLB formation, incubation and washing. 100 μL of SUV solution was deposited on top of the mica. 2 μL of 0.1 M $CaCl_2$ was added to promote vesicle bursting, followed by the addition of 600 μL of buffer (10 mM HEPES and 150 mM NaCl). 9 μL of 0.01 mM CTxB-Alexa 488 was added only to the SLBs containing GM1 to label the L_o phase domains. The two-color labelling (DOPE-Atto 633 for the L_d phase and GM1 CTxB-Alexa 488 complex for the L_o phase) was used only for the preparation of the representative images to ensure the reader that the membranes were free of holes and defects in both the L_d and L_o phases at each hydration level. All other data (fluorescence and AFM) were acquired on SLBs labelled with the L_d phase probe only to exclude the potential impact of GM1 on the membrane response to dehydration. The sample was incubated for 40 min and then washed to remove the excess vesicles with a total of 20 ml of Milli-Q water. Unless otherwise stated, Milli-Q water was used instead of HEPES buffer for washing to avoid the possible formation of salt crystals on top of the membrane during dehydration. After the final washing step, the Eppendorf tube was gently removed and the sample was transferred to the AFM holder, which was then filled with Milli-Q water to allow proper hydration. For measurements under different hydration conditions, the bulk water was gently removed with a pipette and the sample was mounted in the coverslip holder. Nitrogen gas at >90% RH was immediately flushed through the two ports of the AFM holder.

2.4 Hydration control

Control over the membrane hydration state was done using a home-made control unit as previously described.[37] The relative humidity (RH) of nitrogen gas was adjusted and maintained by mixing wet (saturated with water vapour, 95% RH) and dry (~5% RH) N_2 gas. The final relative humidity and temperature of the N_2 gas were continuously monitored using an electronic thermohygrometer in a range of 0–95% RH and an accuracy of 1%. Samples were exposed to a RH of 90% (62×10^{19} water molecules per min), 70% (48×10^{19} water molecules per min), 50% (34×10^{19} water molecules per min), and 30% (20×10^{19} water molecules per min), and completely dry conditions (~5% RH) during dehydration and rehydration cycles. It should be noted that although the relative humidity of the environment in which the SLB is placed is not a direct property of the lipid membrane, we present our results in terms of RH throughout the manuscript because this is the parameter that we directly controlled in the experiments. However, the environmental RH can be directly translated into a hydration state of the lipid membrane, expressed in terms of the number of water molecules per lipid molecule, as shown in previous works.[37,40,41] Briefly, the conversion is based on the experimental data of Hristova *et al.* (X-ray diffraction) and of Piatkowski *et al.* (infrared spectroscopy), which showed that stacked DOPC lipid bilayers equilibrated at 95% RH contain approximately 11–12 water molecules per lipid in their first hydration shell.[40,41] Lower RH values of 75, 50, and 25% correspond to approximately 6.3, 3.6, and 2.4 water molecules per lipid, respectively. SLBs were incubated at each hydration state for approximately 30 min prior to imaging to ensure proper equilibration of the membrane.

2.5 AFM imaging

AFM measurements were performed using a NanoWizard III system from JPK Instruments, Berlin, Germany, mounted on a Zeiss LSM 510 Meta fluorescence microscope. Measurements were performed using a Biolever Mini cantilever (BL-AC40TS-C2) from Olympus, Tokyo, Japan. Images were acquired in contact mode using a silicon tetrahedral tip with a radius of 10 nm and a spring constant of 0.09 N m^{-1}. The scan rate was set to 1–2 Hz. The force was kept as low as possible. Both topography and deflection (error) signals were measured simultaneously for the trace and retrace directions. The images were post-processed by applying line fitting, which corrects for the offset within the image, using JPK processing software from JPK Instruments, Berlin, Germany. Final image analysis was performed using ImageJ[42] and Gwyddion software.[43] Height mismatch between phases was determined by analyzing height distribution histograms.

2.6 Line tension calculation

Line tension was calculated based on the theoretical model developed by Cohen *et al.*, in which the line tension is directly related to the height mismatch between the L_o and L_d phases:[14]

$$\gamma = \frac{\sqrt{B_s K_s B_r K_r}}{\sqrt{B_r K_r} + \sqrt{B_s K_s}} \cdot \frac{\delta^2}{{h_o}^2} - \frac{1}{2} \cdot \frac{(J_s B_s - J_r B_r)^2}{\sqrt{B_r K_r} + \sqrt{B_s K_s}} \quad (1)$$

where γ is the line tension, δ is the phase height mismatch, h_o is the monolayer thickness, B is the elastic splay modulus, K is the tilt modulus and J is the spontaneous curvature of the monolayer. The monolayer thickness is defined as an average thickness of L_d (h_s) and L_o phase (h_r) monolayers:

$$h_o = \frac{(h_r + h_s)}{2} \quad (2)$$

Following the model assumptions presented by García-Sáez *et al.*, we considered the values of $B_r = B_s = 10$ kT, $K_r = K_s = 40$ mN m^{-1}, and $J_r = J_s = 0$, which describe the scenario of "soft" domains.[16] We determined that the thickness of the DMoPC bilayer (L_d phase) measured at 90% RH was 3.87 ± 0.21 nm, while the thickness of the L_o phase was calculated by adding the value of the height mismatch between the two phases to the height of the L_d phase.

2.7 Confocal imaging

Confocal imaging for sample localisation prior to AFM measurements was performed on a Zeiss LSM 510 Meta Carl Zeiss, Jena, Germany, using a 20x, 0.75NA objective. Confocal images were obtained by using the excitation light from a He–Ne laser at 633 nm for Atto 633 and an Ar laser was used for excitation of Alexa Fluor 488. Emission was collected in the wavelength range of 645–797 nm for the red light channel (Atto 633 detection) and 495–530 nm for the green light channel (Alexa Fluor 488). High quality images were obtained by using a Zeiss 710 microscope with a 40× 1.3 NA oil immersion objective. Minimal laser power was used in all imaging experiments to minimise photobleaching. To quantify the shape of the lipid domains based on the confocal images obtained at different hydration states, the circularity parameter was calculated as follows:

$$\text{circularity} = 4\pi \frac{\text{area}}{\text{perimeter}^2} \quad (3)$$

Image processing and calculation of domain circularity were done using ImageJ/Fiji software.[44]

3 Results and discussion

3.1 Analysis of fluorescence in dehydrated lipid membranes

Nanoscale characterisation of the supported lipid bilayers (SLBs) in different hydration states has been carried out for membranes reconstituted from a ternary lipid mixture of DMoPC/SM/cholesterol in a molar ratio of 1 : 1 : 1. This membrane composition leads to the formation of L_o domains enriched in sphingomyelin and cholesterol embedded in the L_d phase composed of more loosely packed PC lipids. The structure of the membranes with this lipid composition has been well characterised in the literature in terms of domain size and shape[16] and membrane dynamics[45] under conditions of full hydration, where the membrane is embedded in an aqueous environment. In contrast, here we focused on elucidating the structural properties of lipid bilayers in a wide range of hydration states: from full hydration (bulk hydration) to dry membranes containing only a few water molecules per lipid. The degree of membrane hydration was tuned and controlled using the previously described humidity control setup schematically shown in Fig. 1a, in which water-enriched nitrogen is supplied directly to the membrane (see Materials and methods).[37] The coupling of a confocal microscope with an AFM system allowed the simultaneous observation of microscale and nanoscale changes in the lateral organisation of the membrane as a function of its hydration state. Analysis of the fluorescence images showed that the overall membrane structure was unaffected by dehydration. Despite the small number of vesicles and aggregates that were deposited on top of the bilayer during dehydration, the membrane remained intact with readily distinguishable phase separation.

However, as the hydration of the membrane is reduced, small changes in the shape of the L_o domains become apparent in the form of a more jagged perimeter of the L_o phase domains, as shown in Fig. 1b. To provide quantitative information about these differences in the domain shape, we calculated the circularity parameter by analysing all clearly resolvable domains from at least four images of two different samples. The domain circularity decreased with decreasing humidity, as shown in Fig. 2a. Under fully hydrated conditions the domain circularity was 0.82 ± 0.02, while at 5% RH it decreased to 0.51 ± 0.01. To verify that the changes in domain circularity were caused solely by the hydration state of the membrane, we performed additional experiments, where after 0.5 h of incubation time at 70% RH, the membrane was monitored for a further 0.5 h under exactly the same humidity conditions to record any potential changes in the shape and circularity of the L_o phase domains. As shown in Fig. S1a and b,† there were no visible changes in the shape or distribution of the domains. Quantitative analysis confirmed this result (Fig. S1c†) – the calculated circularity parameters were the same: 0.61 ± 0.07 and 0.63 ± 0.07, measured immediately after sample equilibration to 70% RH and after 30 min of further incubation under the same humidity conditions, respectively. It should be noted that the subsequent restoration of high membrane hydration led to the reappearance of domain circularity. The domain circularity values corresponding to the specific hydration levels were the same for the dehydration and rehydration trajectories within the range of 5–70% RH. However, at 90% RH during the rehydration cycle, the domain circularity decreased to a value of 0.53 ± 0.03 (see the purple triangle in Fig. 2a). As shown in Fig. S2a and b,† we observed that at this value of environmental humidity, the domains largely merged and formed elongated structures composed of a few integrated domains, leading to a significant decrease in the circularity parameter. In agreement with our previous reports, under high humidity conditions the lipids regain their initial mobility, which favours the merging of the lipid domains.[37] In addition to the global analysis (of the entire images) of the circularity of the L_o phase at 90% RH, we also analysed 25 domains that did not undergo merging (see Fig. S2c†) and observed that their circularity regained the initial value upon rehydration.

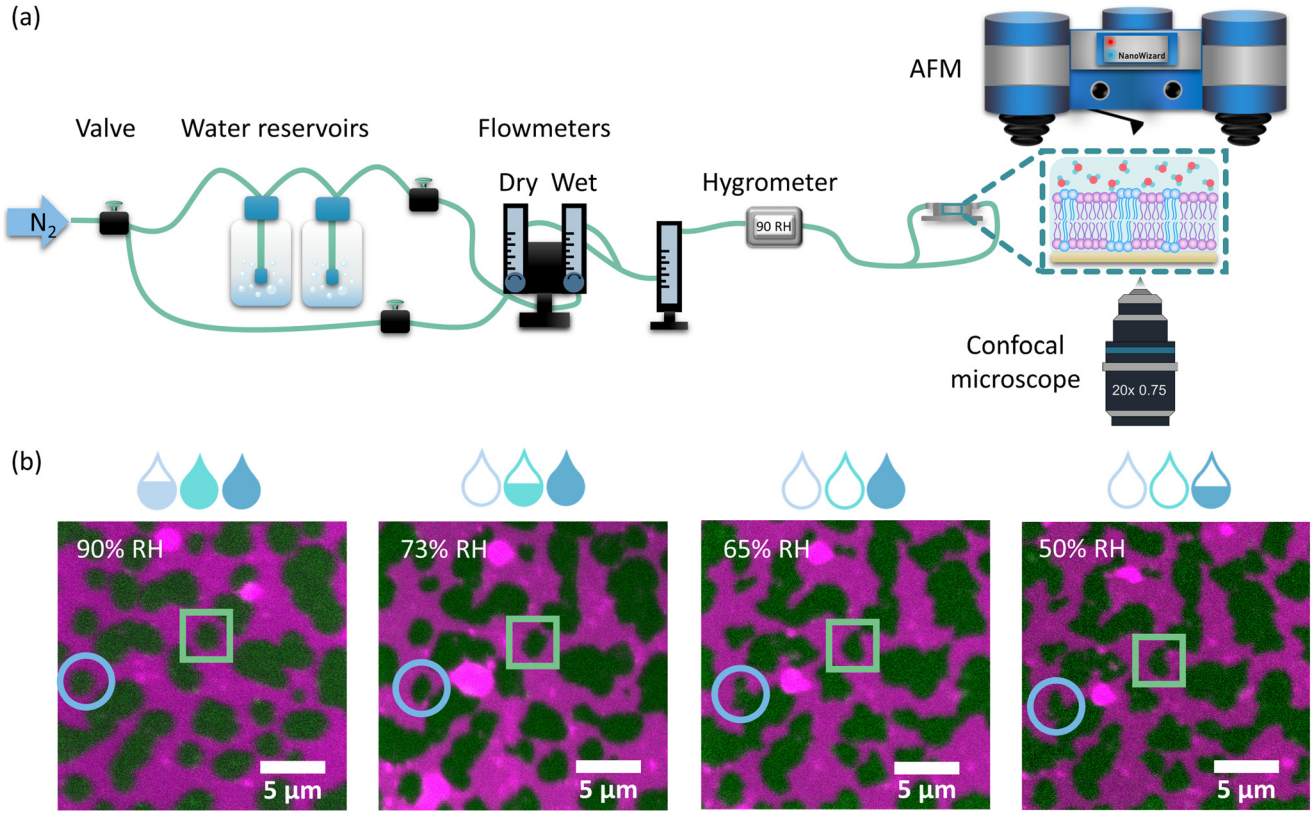

Fig. 1 (a) Schematic representation of the home-built humidity control setup, which allows simultaneous AFM and confocal measurements of biomimetic cell membranes under varying hydration conditions. The setup consists of a source of nitrogen gas (N_2), two reservoirs of water, 3 flow meters, providing information on the dry, wet and final flow reaching the sample, 3 manual valves for precise control of the flow rate, and an electronic thermohygrometer. (b) Fluorescence images of the representative SLB showing phase separation into L_d (labelled with DOPE-Atto 633, shown in magenta) and L_o (labelled with CTxB-Alexa 488, shown in green) domains under different hydration conditions of: 90% RH, 73% RH, 65% RH, and 50% RH. Domains of the L_o phase become less circular with decreasing hydration level (see, *e.g.* domains indicated by blue circles and green squares). Experiments were carried out in 10 mM HEPES and 150 mM NaCl buffer.

The observed changes in the shape of the L_o domains suggest an increased miscibility of the lipids composing both phases. If indeed true, this could also be manifested in the fluorescence signal, as one would expect higher L_d label fluorescence intensity within the L_o phase, due to lipid admixing. To monitor whether the compositional changes occurred within the domains of the L_o phase, we measured the average fluorescence intensity of the L_d phase labelling dye DOPE-Atto 633 within the domains (I_D) and divided this by the average intensity of this dye at 1 µm from the domain boundary (I_N). By taking the ratio (I_D/I_N) of the fluorescence intensities measured within the L_o domain and immediately adjacent within the L_d phase, we ensure that any potential mechanisms affecting the detected fluorescence signal of the dye in both phases, such as for instance a change in the quantum efficiency of the dye or focusing of the objective (hence the fluorescence collection efficiency), are divided out. Interestingly, we observed more than a 3-fold increase in the I_D/I_N ratio for the membranes equilibrated at 90, 70, 50, 30, and 0% RH compared to the membrane containing bulk water as shown in Fig. 2b. Upon dehydration, there was a clear increase in the fluorescence intensity of DOPE-Atto 633 within the L_o domains. The observed increase in fluorescence may in principal be due either to the increased migration of lipids from the L_d phase to the L_o phase or to changes in the photophysical properties of the label fluorophore. To investigate this, we performed additional control experiments and determined the changes in the fluorescence intensity as a function of membrane hydration for a single component, non-phase separated SLB composed of 14 : 1 PC doped with 0.1 mol% of DOPE-Atto 633 (please see ESI note 1 and Fig. S3† for control experiments and further discussion). We found that dehydration increased the detected fluorescence signal by a factor of approximately 1.6 (Fig. S3a†). Given the very high fluorescence quantum yield (QE) of Atto 633 (64% in water), it is not physically possible that the observed increase is solely due to the increase in the QE of the dye, as this would indicate that the QE increases to a value >100%. It should be noted here that the optical properties of the studied system also change as a function of hydration. In particular, the fluorescence collection efficiency is affected by the refractive index of the medium in which the emitting dipoles are placed.[46] In bulk water, fluo-

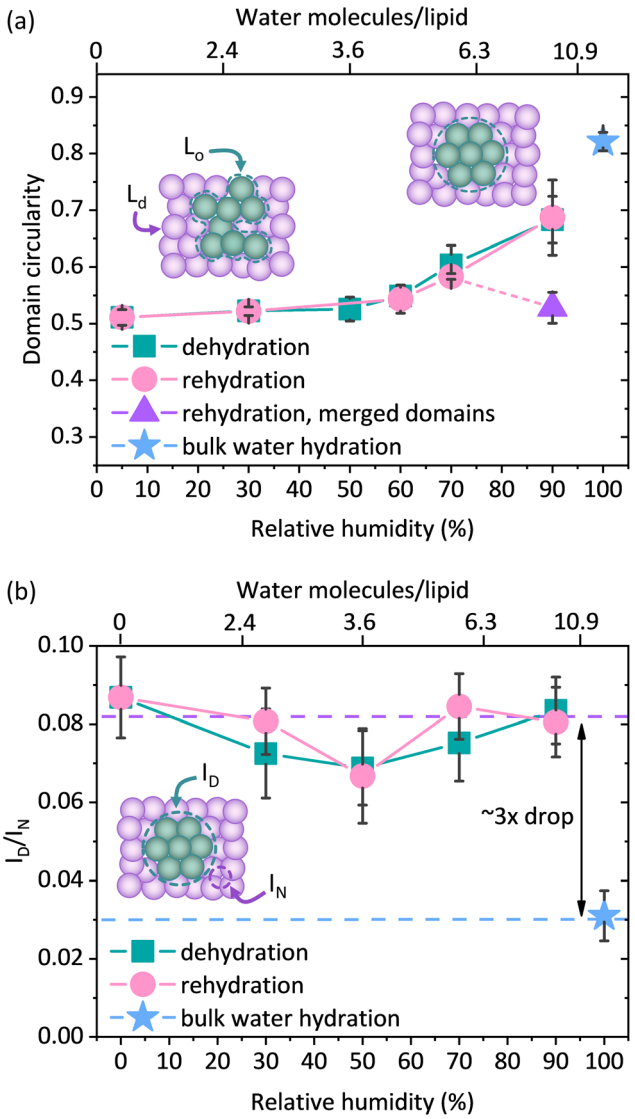

Fig. 2 (a) Circularity of the L_o phase domains calculated from the confocal images for the fully hydrated sample during the cycle of dehydration (90, 70, 60, 50, 30, and 5% RH) and subsequent rehydration (5, 30, 60, 70 and 90% RH). The violet triangle corresponds to the domain circularity calculated for 25 unmerged domains from three different areas. (b) Fluorescence intensity within the domain (I_D) divided by the intensity in the region adjacent to the domain (I_N) as a function of membrane hydration. Experiments were performed in buffer containing 10 mM HEPES and 150 mM NaCl. Four different areas (size 50 × 50 μm) of 2 individual SLBs were analysed. Each area contained approximately 200 domains. The bottom *x*-axis shows the values of relative humidity, which can be correlated with the number of water molecules per lipid (see the upper *x*-axis).

rescence is emitted more symmetrically with respect to the substrate plane, whereas under dehydrated conditions, fluorescence is emitted predominantly towards the substrate. Thus, the observed increase in the fluorescence intensity of DOPE-Atto 633 in the single component membrane most likely includes a contribution from the optical effects. Regardless of the exact contributions of the effects discussed above (which are very difficult, if not impossible, to disentangle), we clearly observed (Fig. S3b†) that the fluorescence signal of Atto 633 increases much less in the L_d phase (~×1.5) than in the L_o phase (~×4.7). In fact, if the redistribution of DOPE-Atto 633 were the only (or main) mechanism, then one should observe an increase in the fluorescence intensity in the L_o domain and a decrease (by the same absolute amount) in the fluorescence intensity in the adjacent L_d phase area. Indeed, if we correct the observed increase in fluorescence intensity in the L_o/L_d phases by a factor of 1.6, determined from the single-component membrane, we found (Fig. S3c†) that the fluorescence intensity in the L_o phase increases by approximately 600 counts, whereas in the L_d phase we observed a decrease in fluorescence intensity by approximately 600 counts. The observed changes, *i.e.* the decrease in fluorescence in the L_d phase and the increase in fluorescence in the L_o phase, correlate very well. All the evidence suggests that the observed 3-fold increase in fluorescence intensity is due to the diffusion of the Atto dye-carrying lipids from the disordered to the ordered phase.

Altogether, the analysis of domain circularity and fluorescence intensity within the L_o domains consistently points toward the enhanced lateral reorganisation of the membrane constituents under dehydration conditions. The size of the ordered phase domains in this study was approximately 1–5 μm^2, so the details of the structural reorganisation are hidden below the resolution limit of the fluorescence microscope and could not be resolved based on the fluorescence signal.

3.2 Nanoscale structural changes under dehydration conditions

The macroscopic structural analysis of the SLBs under different hydration conditions suggests a structural rearrangement of the lipids at the nanoscale. To identify the exact origin of the observed changes within the lipid domains, we used AFM imaging. A home-built hydration setup was connected directly to the AFM JPK coverslip holder *via* perfusion inlets, allowing for continuous gas flow within the chamber, as shown in Fig. 1a. In the presence of excess water, we observed a well-defined phase separation as shown in Fig. 3a (bulk water). The unlabelled areas measured by confocal microscopy corresponded to the more protruding regions detected by AFM and are identified as L_o phase lipid domains.[47] Lipid domains under fully hydrated conditions had a round shape with smooth edges. Upon removal of bulk water and a subsequent gradual decrease in membrane hydration, the boundaries between the L_o and L_d phases became jagged, as shown in Fig. S4† (90–5% RH). At the same time, we observed the formation of small areas of lower height, which we attributed to the L_d phase nanodomains formed within the L_o phase domains, reminiscent of admixing phenomena recently observed for similar mixtures of photoswitchable lipids.[48,49] Measurements immediately after the removal of bulk water required constant adjustment of the applied force and performing of many scans to remove aggregates deposited on top

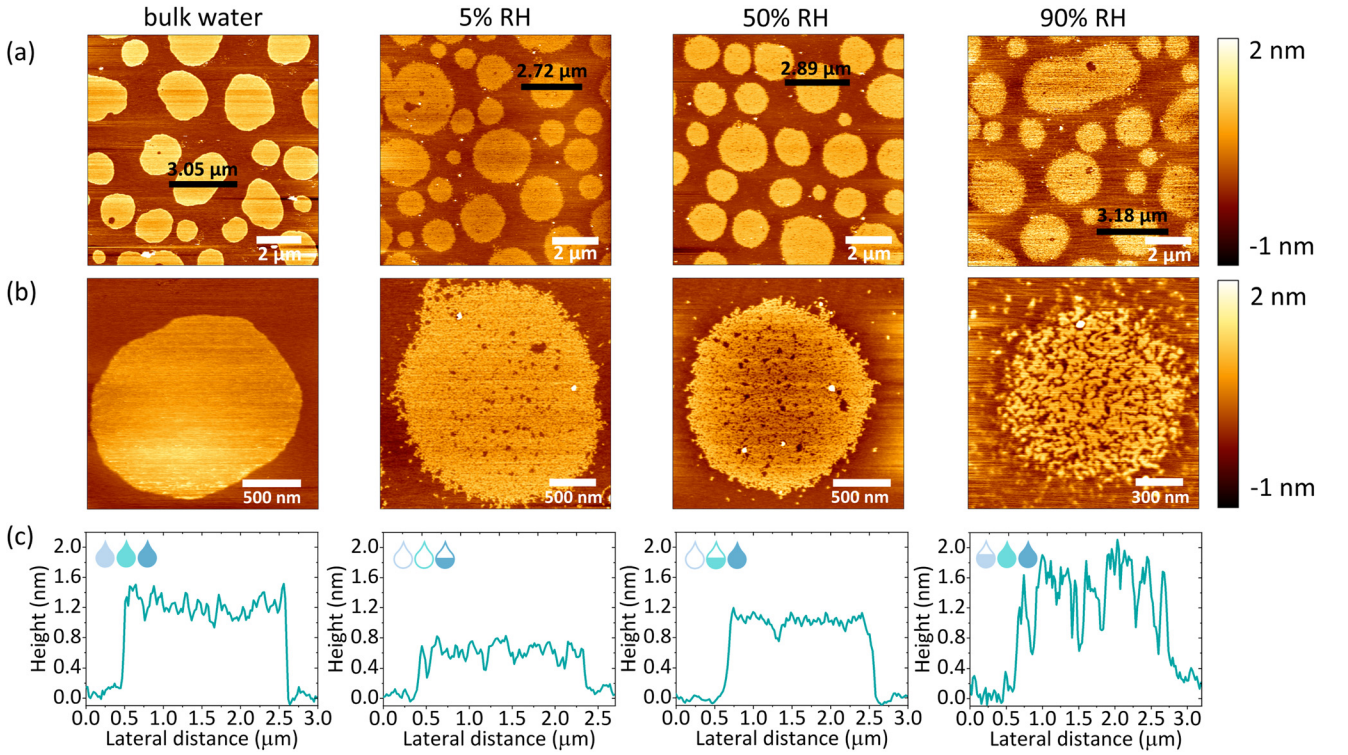

Fig. 3 (a) Representative images of the fully hydrated SLB and SLBs after removal of bulk water and equilibrated at 5, 50 and 90% RH. (b) High-resolution images of single domains at different hydration levels (bulk water hydration, 5, 50 and 90% RH). (c) Height profiles corresponding to the black horizontal lines shown in (a).

of the membrane. In addition, at high humidity, the membrane is very sticky and adheres to the AFM tip during scanning, which can drag membrane fragments as shown in Fig. S5.† Consequently, measurements at high humidity levels required constant changing of the measured spot, thus during the dehydration cycle (Fig. S4†) we did not follow the structural reorganization of the membrane in the exact same area but rather focused on the global characterisation of the sample.

It should be emphasised that a gradual decrease in hydration did not lead to such a pronounced reorganisation of the domain shape (domain boundary) throughout the dehydration and rehydration cycles, as it was observed in the case of confocal imaging. From our previous studies, it is clear that as hydration decreases, the diffusion of lipids, as well as their mobile fraction, decreases abruptly when the number of water molecules hydrating the membrane falls below a certain value.[37,50] At 50% RH and below, the mobility of lipids is almost completely ceased, due to the breaking of the first hydration shell surrounding a single lipid head group moiety. In addition, other recent studies of ours have shown that the dynamics of lipids under dehydration conditions is strongly influenced by the ionic composition of the buffer hydrating the membrane.[51] Although lipids remain mobile in the presence of Na^+ ions at humidity above 50% RH, their mobility is significantly reduced in MilliQ water upon dehydration to 85% RH. In the course of the measurements presented here, we decided to perform AFM scanning in the absence of salt-enriched buffer, which could lead to salt crystallisation on the membranes. Therefore, membranes prepared in HEPES buffer, were thoroughly washed with MilliQ water to remove any residual salt. The absence of Na^+ ions in the residual water leads to lower (<0.2 $\mu m^2\ s^{-1}$) lipid mobility under reduced hydration conditions, explaining the lack of macroscopic circularity changes within the membranes at low humidity. However, it should be noted that although lipid mobility is affected under dehydration conditions, there was a noticeable structural reorganisation in the partially dehydrated membrane compared to the membrane under fully hydrated conditions.

After dehydration, a gradual rehydration of the membrane was performed to confirm the complete preservation of the structure throughout the entire cycle of lowering and raising the humidity. As shown in Fig. 3a and S6a,† throughout the entire rehydration process the integrity of the lipid membranes remained intact. Iriarte-Alonso *et al.* reported that pure DOPC membranes lose their structural arrangement and membrane continuity upon abrupt and complete dehydration and rehydration, resulting in an abundance of various defects and holes exposing the bare support.[31] This gives even more importance to the dehydration method presented in our research, which allows the membrane and lipids to adapt to the slowly changing hydration state of the membrane. The high resolution images of individual domains revealed increased mixing of the L_o and L_d phases as shown in Fig. 3b and S6b.† As

shown in Fig. 3c, the AFM height profiles across the domains showed that the height mismatch between the L_d and L_o phases was different under different hydration conditions. Thus, we concluded that the more pronounced phase mixing at higher hydration values was due to two phenomena: (i) the gradual recovery of lipid mobility, leading to a more dynamic membrane reorganisation and (ii) the increase in hydrophobic mismatch between phases, promoting phase separation. Consequently, the lipids of the L_d phase separate from the L_o phase and merge to minimise the perimeter exposed to water (see Fig. S7†).

Based on the AFM images, we determined the total bilayer thickness for the membrane without bulk water (90% RH) by selecting areas with membrane defects as shown in Fig. 4a. The formation of holes was induced by applying an abrupt dehydration procedure, which is based on the rapid aspiration of water with a pipette. Moreover, in order to find ruptured parts of the membrane, we selected areas near the edges of the solid substrate, which are more susceptible to the air–water interfacial peeling force acting during dehydration. We extracted cross-sectional profiles over the areas containing three types of features: holes, and L_o and L_d phases, and found that the height difference between the L_d phase and the surface of the bare substrate was 3.87 ± 0.21 nm, which we attributed to the thickness of the DMoPC bilayer. It should be noted that this value is in agreement with the bilayer thickness of 3.86 nm reported by Lee *et al.* for a fully hydrated membrane also composed of DMoPC lipids.[52] From the height profiles, it was possible to distinguish the domains of the L_o phase protruding approximately 1.3 nm from the L_d phase. Furthermore, the height profiles along the domains confirmed that the intermediate height regions represent the L_d phase trapped within the L_o domains, as the height difference obtained corresponds to the L_o/L_d height mismatch (see Fig. 4b).

3.3 Hydrophobic mismatch and line tension under dehydration conditions

The preparation of lipid membranes from the ternary lipid mixture used in this study results in the formation of lipid domains composed of the L_o phase embedded in the L_d lipid matrix. AFM[53,54] and X-ray scattering[55,56] studies clearly show that the L_o phase, due to the presence of saturated and more densely packed lipids, is thicker than the L_d phase which contains unsaturated lipids. This results in the so-called "height mismatch" or "hydrophobic mismatch" between the two phases. Although this height difference is well defined for SLBs composed of phospholipids with different fatty acid chain lengths in bulk water, it has not been measured under reduced hydration conditions due to the problems in maintaining the structural integrity of the membrane during desic-

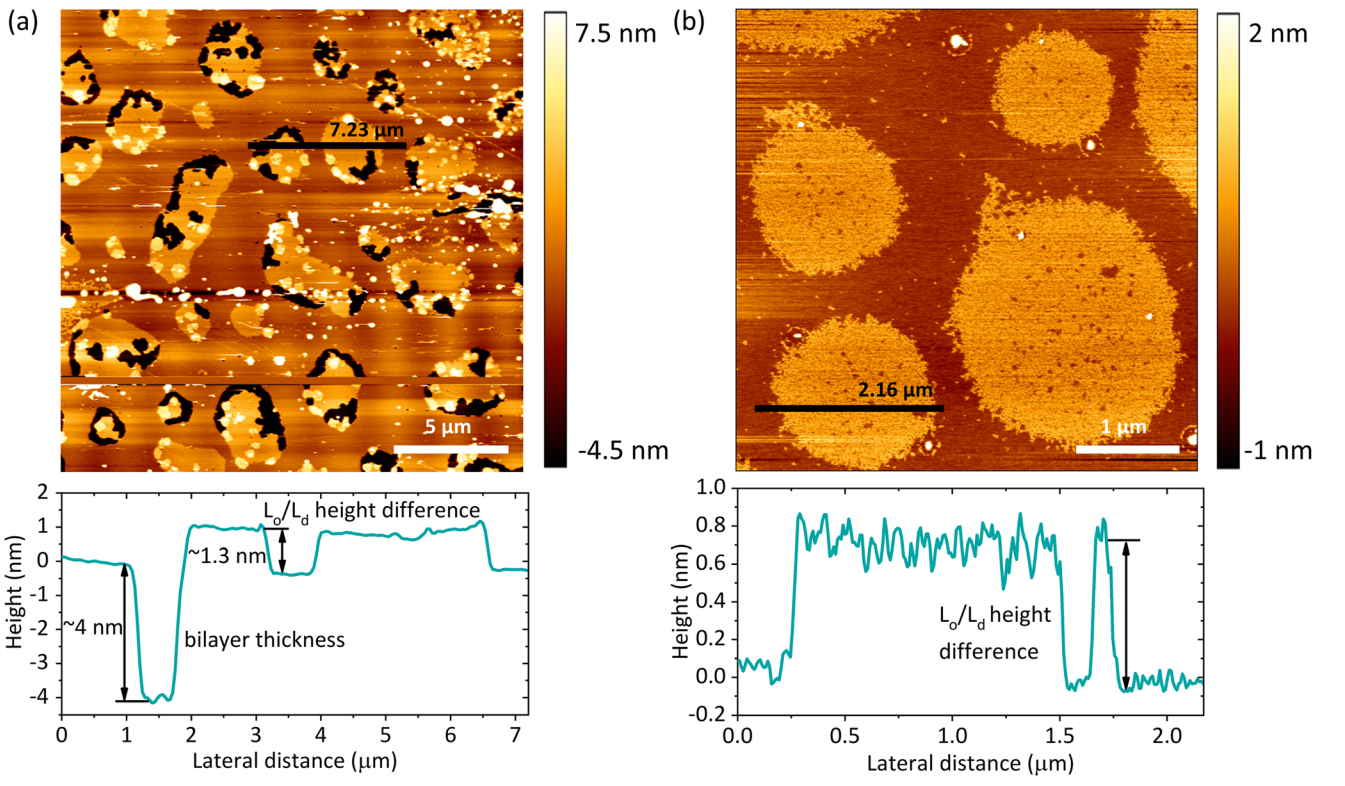

Fig. 4 (a) SLB after abrupt removal of bulk water and subsequent equilibration at 90% RH. The bilayer thickness at 90% RH was approximately 4 nm with a height difference between the L_o and L_d phases of approximately 1.3 nm. (b) SLB after careful removal of bulk water and subsequent equilibration at 5% RH. The intermediate height regions within the L_o phase domains correspond to the L_d phase. The height difference between the phases under these hydration conditions was about 0.8 nm.

cation.[16] From the height distribution histograms (see Fig. S8†), we determined the height mismatch between phases in a wide range of membrane hydration states, as shown in Fig. 5a. We observed that the height mismatch decreased from 1.36 ± 0.19 nm at 90% RH to 0.8 ± 0.04 nm at 5% RH during dehydration. These changes were almost completely reversible upon rehydration. Importantly, measurements in bulk water and under all hydration conditions were made with the same cantilever and in one mode (contact mode) to ensure that the values obtained were comparable. The sudden increase in the height mismatch observed when going from bulk hydration (100% RH) to 90% RH is an experimental artifact due to abrupt changes in the balance between attractive and repulsive forces to which the AFM tip is subjected immediately after the removal of bulk water (see ESI note 2†).

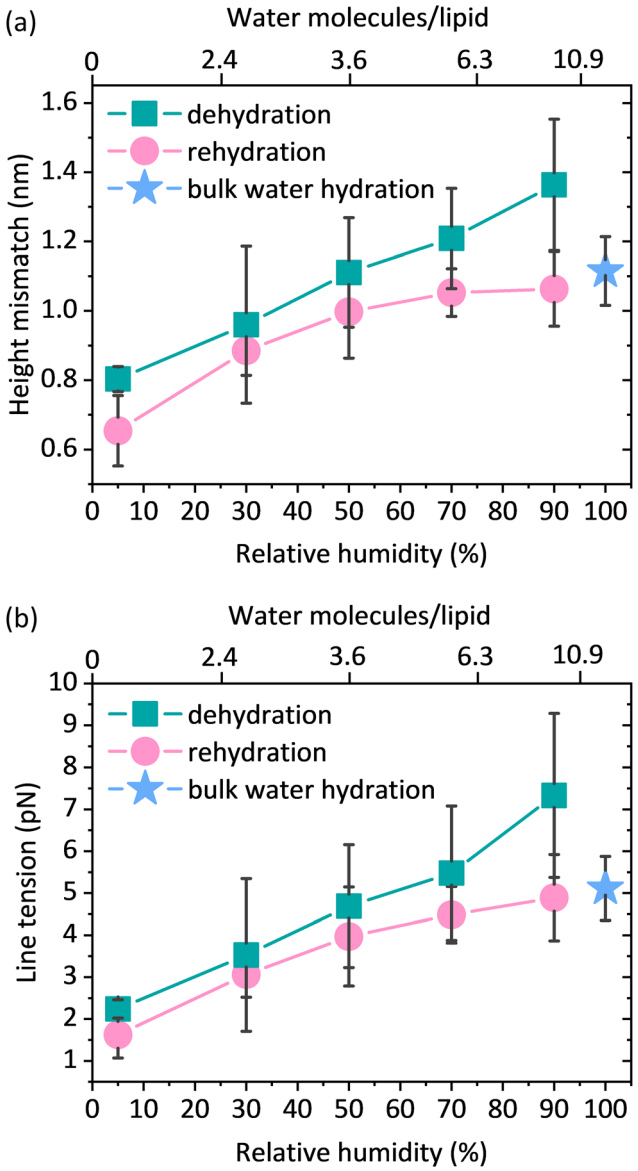

Fig. 5 (a) Height mismatch between the L_o and L_d phases during dehydration and rehydration analysed from the height histograms of 3–8 different images containing multiple domains of the L_o phase. (b) Line tension during dehydration and rehydration calculated from the model assuming the presence of soft domains, no spontaneous curvature, and no change in the height of the L_o phase during the hydration change cycle. Height mismatch and line tension were determined from 3–8 images (depending on the hydration level) of 3 individual SLBs; each image contained multiple L_o domains. The bottom *x*-axis shows the values of relative humidity, which can be correlated with the number of water molecules per lipid (see the upper *x*-axis).

The height mismatch between the L_o and L_d phases changes gradually (Fig. 5a). One would therefore expect that with dehydration there should be a steady increase in the number of L_d phase lipids diffusing into the L_o zone. However, in the fluorescence data (Fig. 2b) we observed more of a stepwise behaviour, where after an initial increase in the fluorescence intensity of the L_d phase probe in the L_o domain, we observed a fairly constant intensity at all other humidities. At first glance, it may seem somewhat surprising that the trends in the fluorescence data and the height contrast data are different. However, it is important to note that the changes in the height mismatch are in no way related to the mobility of the lipids. The observed changes in lipid partitioning are associated with the decreased hydrophobic mismatch, but unlike the height mismatch data, they are also strongly dependent on the lipid mobility. Since lipid mobility decreases strongly with decreasing membrane hydration,[37,50,51] it is not too surprising that we do not see a steady increase in the partitioning of the L_d phase lipids into the L_o phase. At lower membrane hydration states, we observed a competition between the lower hydrophobic mismatch, which favours lipid admixing, and the lower diffusivity, which hinders mixing.

The lateral organisation of the membrane, the distribution of the domains, and their size and shape are all driven, among other things, by the height mismatch between the L_d and L_o phases, which is a key factor leading to the occurrence of line tension at the boundary between two phases. Exposure of the hydrophobic tails of the lipids to the aqueous environment is energetically unfavorable. Therefore, the lipids of the L_o phase tend to organise themselves into domains in order to reduce the boundary at the phase interface, thus reducing the exposure to the aqueous medium. The theoretical model developed by Cohen *et al.* showed that the line tension increases quadratically with the phase height mismatch.[14] Experimental work based on this model has shown that by varying the length of the PC acyl chain from 22 to 14 carbons, the height difference between the phases increases from 0.17 ± 0.9 nm to 1.56 ± 0.13 nm, leading to a 100-fold increase in the values of the line tension, from 0.06 to 6 pN, respectively.[16] Line tensions of a similar order of magnitude have also been obtained using other approaches such as the measurement of the domain nucleation rate[57] or the analysis of the vesicle geometry based on the Jülicher and Lipowsky theory.[58] Surprisingly, the line tension in membranes has never been calculated or measured as a function of its main determinant, which is the presence of water. From the extracted profiles for samples at 90% RH, it could be concluded that the total lipid bilayer thickness does not appear to change upon removal of bulk

water, as the bilayer thickness measured at 90% RH of 3.87 nm is consistent with the value of 3.86 nm reported in the literature for a fully hydrated DMoPC bilayer.[52] The determination of the effective thickness of the L_o and L_d phases was not possible for each hydration level, because the lipid membranes did not show any defects in the form of holes and membrane disruptions that would provide the reference plane for height measurements. While it is relatively easy to induce holes in the membrane, as it requires the abrupt removal of bulk water, once membrane defects are formed and the hydration is further gradually reduced, they behave in an unpredictable manner; they rapidly expand in all directions, and the edges of the membrane curl up. This progressive degradation of the membrane makes it difficult to follow the absolute thickness of the bilayer as the hydration changes. However, NMR and X-ray diffraction experiments on the membranes under lower hydration conditions showed that the lipids forming the L_d phase are more susceptible to height changes during dehydration. The lipids of the L_d phase undergo a straightening of the acyl chains, leading to a decrease in the lateral area per lipid molecule and consequently an increase in their hydrophobic thickness.[59,60] Moreover, recent simulation results on the behavior of lipid membranes under reduced hydration clearly show that, in the absence of water, the lipids of the L_d phase undergo a liquid–gel transition and exhibit properties of an ordered membrane, which is stiffer with the acyl chains of the lipids more densely packed.[60] With this in mind, we infer that the change in height mismatch and the consequent change in the line tension are caused by the straightening of the fatty acid chains of the lipids composing the L_d phase, rather than a change in the thickness of the L_o phase. We calculated the line tension using the equation proposed by Cohen *et al.*[14] (see the Materials and methods section), assuming that the difference in height was caused by the increase in the thickness of the L_d phase. We observed that there was a linear dependence of the line tension on the degree of hydration (Fig. 5b).

While all the evidence discussed above suggests that it is the L_d phase that changes its height when the membrane hydration is altered, we also considered two other scenarios, in which a decrease in the hydrophobic mismatch is caused by a decrease in the thickness of the L_o phase or by both phases having the opposite effect, *i.e.* the thickness of the L_d phase increases with a simultaneous decrease in the thickness of the L_o phase (see Fig. S9a†). Regardless of the assumptions, for all three scenarios we observed the same trend in the changes of the line tension at varying hydration levels, *i.e.* an almost 3-fold decrease of the line tension for the lowest humidity of 5% RH when compared to 90% RH (see Fig. S9b and S9c†).

4 Conclusions

In this paper, we have presented a methodology for AFM measurements under varying hydration conditions, in which biomimetic membranes are directly subjected to the slow gradual changes of their hydration state. The phase-separated lipid membranes, characterised by the presence of the L_d and L_o phases, were exposed to a wide range of environmental humidities and fluorescence images as well as membrane topography information were acquired simultaneously. We observed that the overall lateral organisation of the lipid membranes, *i.e.* the presence of phase separation and the continuity of the structure, did not change upon removal of bulk water and subsequent gradual dehydration of the membrane. However, the absence of bulk water leads to an increased miscibility of the lipids constituting the L_d phase within the domains of the L_o phase, as compared to fully hydrated conditions. We investigated the response of biomembranes to the dehydration conditions in terms of the line tension, which has only been measured as a function of lipid chain length and never through the direct effect of water content. We observed a 3-fold difference in the line tension between the two extreme hydration states. The significant drop in line tension at the L_d and L_o phase interface explains the tendency of lipids from different phases to mix more freely at reduced membrane hydration.

Local dehydration of two merging cell membranes is an indispensable prerequisite for all fusion events that occur during biological processes such as viral entry, endo- and exocytosis, neurotransmission or fertilisation. Fusion can be modulated in two ways: using different types of fusogenic proteins, such as SNAREs, or by structural, local adaptation of the membrane lipid composition.[61] It has been shown that cholesterol accumulates in the regions of high curvature during stalk formation in fusion events.[62] This is attributed to the ability of cholesterol to increase the membrane fluidity and induce the formation of negative curvature. Sphingomyelin is known to promote the formation of a denser and less fluid L_o phase, effectively inhibiting the membrane fusion.[63] The opposite effect is induced by unsaturated lipids, which form the L_d phase, stimulating membrane curvature and promoting the formation of fusion intermediates.[64] Although the fusion of two membranes preferentially occurs in the regions of high fluidity, viral protein elements such as HIV fusion peptides have been shown to bind to high line tension L_o–L_d interface regions, where they promote the membrane fusion of the HIV viral envelope with the host cell membrane.[65] The revised stalk–pore model, extended to heterogeneous membranes (exhibiting L_o–L_d phase coexistence), proposes that the reduction of line tension at the lipid phase boundary during stalk formation generates additional energy for the fusion, facilitating viral entry through phase boundary regions.[66] As we have shown here, the reduction in line tension under dehydration conditions is associated with an extensive lipid migration between the L_d and L_o phases. It is therefore possible that the observed changes in local membrane fluidity and flexibility, as well as the reduced line tension, are yet another factor required for the fusion to occur.

While partial dehydration of the membranes has been presented as an inherent requirement for the mechanism of membrane fusion, the term 'dehydration' is far from well

defined, as it is not clear to what extent membranes actually become dehydrated. One way of describing membrane dehydration would be to define a state where the amount of hydrating water decreases to a level where the dynamic or structural properties of the membrane begin to be affected. Based on the experiments reported here as well as our recent works,[37,50,51] both the dynamics and the structure of the membrane are gradually affected when the first hydration shell of the lipids is perturbed. In the case of the zwitterionic phosphocholine lipids, this happens when the hydration drops below about 12 molecules per lipid. Thus, the thickness of the water layer is at most 1–2 monolayers of water on top of the membrane. This suggests that biomimetic membranes don't really 'feel' any changes in hydration properties beyond their first hydration shell. Certainly, it would be fascinating to monitor membrane's properties while controlling the thickness of the hydrating water layer from a few nanometers all the way down to a few water molecules per lipid, in the regime that is directly relevant to the mechanism of membrane fusion, but the question of how to control the thickness of the hydrating layer beyond the first hydration shell remains open.

In conclusion, our results provide new insights into the behavior of biological membranes under water shortage conditions in terms of their lateral organisation and adaptation to membrane dehydration. The results presented here bring a new perspective to the processes that require local membrane dehydration, such as cell fusion, fertilisation or binding of macromolecules. Finally, the methodology proposed in this research for AFM measurements in varying hydration states provides new possibilities for studying other biological systems and their interactions with water.

Author contributions

Emilia Krok: conceptualization, validation, investigation, writing – original draft, visualization, and funding acquisition. Henri G. Franquelim: conceptualization, validation, investigation, resources, and writing – review and editing. Madhurima Chattopadhyay: conceptualization, validation, and writing – review and editing. Hanna Orlikowska-Rzeznik: validation and writing – review and editing. Petra Schwille: writing – review and editing, resources, and supervision. Lukasz Piatkowski: conceptualization, validation, supervision, writing – original draft, and funding acquisition.

Conflicts of interest

There are no conflicts to declare.

Acknowledgements

The authors acknowledge the financial support from the EMBO Installation Grant 2019 (IG 4147). LP acknowledges the financial support from the First TEAM Grant No. POIR.04.04.00-00-5D32/18-00 provided by the Foundation for Polish Science (FNP). EK acknowledges the financial support from the Ministry of Education and Science of Poland in the year 2022 (Project No. 0512/SBAD/6212). HOR acknowledges the financial support from the National Science Centre (Poland) through OPUS grant, project no. 2020/37/B/ST4/01785.

References

1 J. Lombard, Once upon a Time the Cell Membranes: 175 Years of Cell Boundary Research, *Biol. Direct*, 2014, **9**, 32.
2 N. J. Yang and M. J. Hinner, Getting across the Cell Membrane: An Overview for Small Molecules, Peptides, and Proteins, *Methods Mol. Biol.*, 2015, **1266**, 29–53.
3 L. Schoonen and J. C. M. Van Hest, Compartmentalization, Approaches in Soft Matter Science: From Nanoreactor Development to Organelle Mimics, *Adv. Mater.*, 2016, **28**, 1109–1128.
4 J. A. Jackman and N. J. Cho, Supported Lipid Bilayer Formation: Beyond Vesicle Fusion, *Langmuir*, 2020, **36**, 1387–1400.
5 L. Picas, F. Rico and S. Scheuring, Direct Measurement of the Mechanical Properties of Lipid Phases in Supported Bilayers, *Biophys. J.*, 2012, **102**, L01–L03.
6 A. E. Vallejo and C. A. Gervasi, Impedance Analysis of Ion Transport through Gramicidin Channels in Supported Lipid Bilayers, *Bioelectrochemistry*, 2002, **57**, 1–7.
7 E. London, Insights into Lipid Raft Structure and Formation from Experiments in Model Membranes, *Curr. Opin. Struct. Biol.*, 2002, **12**, 480–486.
8 J. M. Crane and L. K. Tamm, Fluorescence Microscopy to Study Domains in Supported Lipid Bilayers, *Methods Mol. Biol.*, 2007, **400**, 481–488.
9 E. Krok, M. Stephan, R. Dimova and L. Piatkowski, Tunable Biomimetic Bacterial Membranes from Binary and Ternary Lipid Mixtures and Their Application in Antimicrobial Testing, *Biochim. Biophys. Acta, Biomembr.*, 2023, **1865**(7), 184194.
10 L. J. Pike, Rafts Defined: A Report on the Keystone Symposium on Lipid Rafts and Cell Function, *J. Lipid Res.*, 2006, **47**, 1597–1598.
11 J. D. Nickels and J. Katsaras, Water and Lipid Bilayers, *Subcell. Biochem.*, 2015, **71**, 45–67.
12 F. Martelli, C. Calero and G. Franzese, Redefining the Concept of Hydration Water near Soft Interfaces, *Biointerphases*, 2021, **16**, 020801.
13 P. Jungwirth, Biological Water or Rather Water in Biology?, *J. Phys. Chem. Lett.*, 2015, **6**, 2449–2451.
14 P. I. Kuzmin, S. A. Akimov, Y. A. Chizmadzhev, J. Zimmerberg and F. S. Cohen, Line Tension and Interaction Energies of Membrane Rafts Calculated from Lipid Splay and Tilt, *Biophys. J.*, 2005, **88**, 1120–1133.
15 E. E. Meyer, K. J. Rosenberg and J. Israelachvili, Recent Progress in Understanding Hydrophobic Interactions, *Proc. Natl. Acad. Sci. U. S. A.*, 2006, **103**, 15739–15746.

16 A. J. García-Sáez, S. Chiantia and P. Schwille, Effect of Line Tension on the Lateral Organization of Lipid Membranes, *J. Biol. Chem.*, 2007, **282**, 33537–33544.
17 Y. Zhen, M. Radulovic, M. Vietri and H. Stenmark, Sealing Holes in Cellular Membranes, *EMBO J.*, 2021, **40**, e106922.
18 N. Srividya and S. Muralidharan, Determination of the Line Tension of Giant Vesicles from Pore-Closing Dynamics, *J. Phys. Chem. B*, 2008, **112**, 7147–7152.
19 M. B. Jackson and E. R. Chapman, The Fusion Pores of Ca 2+-Triggered Exocytosis, *Nat. Struct. Mol. Biol.*, 2008, **15**, 684–689.
20 J. Rizo and C. Rosenmund, Synaptic Vesicle Fusion, *Nat. Struct. Mol. Biol.*, 2008, **15**, 665–674.
21 S. C. Harrison, Viral Membrane Fusion, *Nat. Struct. Mol. Biol.*, 2008, **15**, 690–698.
22 P. Primakoff and D. G. Myles, Cell-Cell Membrane Fusion during Mammalian Fertilization, *FEBS Lett.*, 2007, **581**, 2174–2180.
23 R. D. Byrne, S. Veeriah, C. J. Applebee and B. Larijani, Conservation of Proteo-Lipid Nuclear Membrane Fusion Machinery during Early Embryogenesis, *Nucleus*, 2014, **5**, 441–448.
24 G. Shemer and B. Podbilewicz, Fusomorphogenesis: Cell Fusion in Organ Formation, *Dev. Dyn.*, 2000, **218**(1), 30–51.
25 S. Aeffner, T. Reusch, B. Weinhausen and T. Salditt, Energetics of Stalk Intermediates in Membrane Fusion Are Controlled by Lipid Composition, *Proc. Natl. Acad. Sci. U. S. A.*, 2012, **109**, E1609–E1618.
26 S. L. Leikin, M. M. Kozlov, L. V. Chernomordik, V. S. Markin and Y. A. Chizmadzhev, Membrane Fusion: Overcoming of the Hydration Barrier and Local Restructuring, *J. Theor. Biol.*, 1987, **129**, 411–425.
27 S. Aeffner, T. Reusch, B. Weinhausen and T. Salditt, Membrane Fusion Intermediates and the Effect of Cholesterol: An in-House X-Ray Scattering Study, *Eur. Phys. J. E: Soft Matter Biol. Phys.*, 2009, **30**, 205–214.
28 A. Joardar, P. G. Prasad and H. Chakraborty, Mechanism of Membrane Fusion: Interplay of Lipid and Peptide, *J. Membr. Biol.*, 2022, **255**, 211–224.
29 S. Chiantia, N. Kahya and P. Schwille, Dehydration Damage of Domain-Exhibiting Supported Bilayers: An AFM Study on the Protective Effects of Disaccharides and Other Stabilizing Substances, *Langmuir*, 2005, **21**, 6317–6323.
30 M. Del, F. Amalfa, A. M. Nuñez, S. Díaz, A. C. Biondi De Lopez and E. A. Disalvo, Effect of Trehalose and Sucrose on the Hydration and Dipole Potential of Lipid Bilayers, *Biophys. J.*, 2000, **78**, 2452–2458.
31 M. A. Iriarte-Alonso, A. M. Bittner and S. Chiantia, Influenza A Virus Hemagglutinin Prevents Extensive Membrane Damage upon Dehydration, *BBA Adv.*, 2022, **2**, 100048.
32 S. Ohtake, C. Schebor and J. J. de Pablo, Effects of Trehalose on the Phase Behavior of DPPC-Cholesterol Unilamellar Vesicles, *Biochim. Biophys. Acta, Biomembr.*, 2006, **1758**, 65–73.
33 Y. Deng, Y. Wang, B. Holtz, J. Li, N. Traaseth, G. Veglia, B. J. Stottrup, R. Elde, D. Pei, A. Guo and X. Y. Zhu, Fluidic and Air-Stable Supported Lipid Bilayer and Cell-Mimicking Microarrays, *J. Am. Chem. Soc.*, 2008, **130**, 6267–6271.
34 B. P. Oberts and G. J. Blanchard, Formation of Air-Stable Supported Lipid Monolayers and Bilayers, *Langmuir*, 2009, **25**, 2962–2970.
35 R. M. Fabre and D. R. Talham, Stable Supported Lipid Bilayers on Zirconium Phosphonate Surfaces, *Langmuir*, 2009, **25**, 12644–12652.
36 C. T. Han and L. Chao, Creating Air-Stable Supported Lipid Bilayers by Physical Confinement Induced by Phospholipase A2, *ACS Appl. Mater. Interfaces*, 2014, 6378–6383.
37 M. Chattopadhyay, E. Krok, H. Orlikowska, P. Schwille, H. G. Franquelim and L. Piatkowski, Hydration Layer of Only a Few Molecules Controls Lipid Mobility in Biomimetic Membranes, *J. Am. Chem. Soc.*, 2021, **143**, 14551–14562.
38 H. Orlikowska-Rzeznik, E. Krok, M. Chattopadhyay, A. Lester and L. Piatkowski, Laurdan Discerns Lipid Membrane Hydration and Cholesterol Content, *J. Phys. Chem. B*, 2023, **127**, 3382–3391.
39 E. Krok, A. Batura, M. Chattopadhyay, H. Orlikowska and L. Piatkowski, Lateral Organization of Biomimetic Cell Membranes in Varying PH Conditions, *J. Mol. Liq.*, 2022, **345**, 117907.
40 L. Piatkowski, J. De Heij and H. J. Bakker, Probing the Distribution of Water Molecules Hydrating Lipid Membranes with Ultrafast Förster Vibrational Energy Transfer, *J. Phys. Chem. B*, 2013, **117**, 1367–1377.
41 K. Hristova and S. H. White, Determination of the Hydrocarbon Core Structure of Fluid Dioleoylphosphocholine (DOPC) Bilayers by x-Ray Diffraction Using Specific Bromination of the Double-Bonds: Effect of Hydration, *Biophys. J.*, 1998, **74**, 2419–2433.
42 C. A. Schneider, W. S. Rasband and K. W. Eliceiri, NIH Image to ImageJ: 25 Years of Image Analysis, *Nat. Methods*, 2012, **9**, 671–675.
43 D. Nečas and P. Klapetek, Gwyddion: An Open-Source Software for SPM Data Analysis, *Cent. Eur. J. Phys.*, 2012, **10**, 181–188.
44 J. Schindelin, I. Arganda-Carreras, E. Frise, V. Kaynig, M. Longair, T. Pietzsch, S. Preibisch, C. Rueden, S. Saalfeld, B. Schmid, J. Y. Tinevez, D. J. White, V. Hartenstein, K. Eliceiri, P. Tomancak and A. Cardona, Fiji: An Open-Source Platform for Biological-Image Analysis, *Nat. Methods*, 2012, **9**, 676–682.
45 J. Ries, S. Chiantia and P. Schwille, Accurate Determination of Membrane Dynamics with Line-Scan FCS, *Biophys. J.*, 2009, **96**, 1999–2008.
46 D. Axelrod, Evanescent Excitation and Emission, in *Fluorescence Microscopy: Super-Resolution and other Novel Techniques*, Academic Press, 2014, pp. 1–14.
47 E. Sezgin, P. Schwille and T. Dresden, Molecular Membrane Biology Model Membrane Platforms to Study Protein-Membrane Interactions Model Membrane

Platforms to Study Protein-Membrane Interactions, *Mol. Membr. Biol.*, 2012, **29**, 144–154.

48 N. Hartrampf, S. M. Leitao, N. Winter, H. Toombs-Ruane, J. A. Frank, P. Schwille, D. Trauner and H. G. Franquelim, Structural Diversity of Photoswitchable Sphingolipids for Optodynamic Control of Lipid Microdomains, *Biophys. J.*, 2023, **122**(11), 2325–2341.

49 J. A. Frank, H. G. Franquelim, P. Schwille and D. Trauner, Optical Control of Lipid Rafts with Photoswitchable Ceramides, *J. Am. Chem. Soc.*, 2016, **138**, 12981–12986.

50 M. Chattopadhyay, H. Orlikowska, E. Krok and L. Piatkowski, Sensing Hydration of Biomimetic Cell Membranes, *Biosensors*, 2021, **11**(7), 241.

51 M. Chattopadhyay, E. Krok, H. Orlikowska-Rzeznik and L. Piatkowski, Cooperativity between Sodium Ions and Water Molecules Facilitates Lipid Mobility in Model Cell Membranes, *Chem. Sci.*, 2023, **14**, 4002–4011.

52 T. H. Lee, M. A. Sani, S. Overall, F. Separovic and M. I. Aguilar, Effect of Phosphatidylcholine Bilayer Thickness and Molecular Order on the Binding of the Antimicrobial Peptide Maculatin 1.1, *Biochim. Biophys. Acta, Biomembr.*, 2018, **1860**, 300–309.

53 S. Chiantia, N. Kahya, J. Ries and P. Schwille, Effects of Ceramide on Liquid-Ordered Domains Investigated by Simultaneous AFM and FCS, *Biophys. J.*, 2006, **90**, 4500–4508.

54 S. Chiantia, J. Ries, N. Kahya and P. Schwille, Combined AFM and Two-Focus SFCS Study of Raft-Exhibiting Model Membranes, *ChemPhysChem*, 2006, **7**, 2409–2418.

55 T. J. Mcintosh, X-Ray, Diffraction to Determine the Thickness of Raft and Nonraft Bilayers, *Methods Mol. Biol.*, 2007, **398**, 221–230.

56 M. Gandhavadi, D. Allende, A. Vidal, S. A. Simon and T. J. Mcintosh, Structure, Composition, and Peptide Binding Properties of Detergent Soluble Bilayers and Detergent Resistant Rafts, *Biophys. J.*, 2002, **82**, 1469–1482.

57 C. D. Blanchette, W. C. Lin, C. A. Orme, T. V. Ratto and M. L. Longo, Using Nucleation Rates to Determine the Interfacial Line Tension of Symmetric and Asymmetric Lipid Bilayer Domains, *Langmuir*, 2007, **23**, 5875–5877.

58 T. Baumgart, S. T. Hess and W. W. Webb, Imaging Coexisting Fluid Domains in Biomembrane Models Coupling Curvature and Line Tension, *Nature*, 2003, **425**, 821–824.

59 B. W. Koenig, H. H. Strey and K. Gawrisch, Membrane Lateral Compressibility Determined by NMR and X-Ray Diffraction: Effect of Acyl Chain Polyunsaturation, *Biophys. J.*, 1997, **73**, 1954–1966.

60 Y. G. Smirnova, S. Aeffner, H. J. Risselada, T. Salditt, S. J. Marrink, M. Müller and V. Knecht, Interbilayer Repulsion Forces between Tension-Free Lipid Bilayers from Simulation, *Soft Matter*, 2013, **9**, 10705–10718.

61 A. Sardar, N. Dewangan, B. Panda, D. Bhowmick and P. K. Tarafdar, Lipid and Lipidation in Membrane Fusion, *J. Membr. Biol.*, 2022, **255**, 691–703.

62 W. Wang, L. Yang and H. W. Huang, Evidence of Cholesterol Accumulated in High Curvature Regions: Implication to the Curvature Elastic Energy for Lipid Mixtures, *Biophys. J.*, 2007, **92**, 2819–2830.

63 E. Haque, T. J. McIntosh and B. R. Lentz, Influence of Lipid Composition on Physical Properties and PEG-Mediated Fusion of Curved and Uncurved Model Membrane Vesicles: "Nature's Own" Fusogenic Lipid Bilayer, *Biochemistry*, 2001, **40**, 4340–4348.

64 M. Pinot, S. Vanni, S. Pagnotta, S. Lacas-Gervais, L. A. Payet, T. Ferreira, R. Gautier, B. Goud, B. Antonny and H. Barelli, Polyunsaturated Phospholipids Facilitate Membrane Deformation and Fission by Endocytic Proteins, *Science*, 2014, **345**, 693–697.

65 S. T. Yang, V. Kiessling, J. A. Simmons, J. M. White and L. K. Tamm, HIV Gp41-Mediated Membrane Fusion Occurs at Edges of Cholesterol-Rich Lipid Domains, *Nat. Chem. Biol.*, 2015, **11**, 424–431.

66 S. T. Yang, V. Kiessling and L. K. Tamm, Line Tension at Lipid Phase Boundaries as Driving Force for HIV Fusion Peptide-Mediated Fusion, *Nat. Commun.*, 2016, **7**, 11401.